Int. J. Electrochem. Sci., 12 **(2017)** 8421 – 8431, doi: 10.20964/2017.09.50

International Journal of ELECTROCHEMICAL SCIENCE
www.electrochemsci.org

Short Communication

Copper-Doped Iron Carbide as Counter Electrodes for Dye-Sensitized Solar Cells

Haopeng Cai[1,*], *Jie Li*[1,2], *Rui Wang*[2], *Fanglin Wu*[2], *Xing Tong*[1,2]

[1] School of Materials Science and Engineering, Wuhan University of Technology, Wuhan 430070, PR China.
[2] State Key Laboratory of Advanced Technology for Materials Synthesis and Processing, Wuhan University of Technology, Wuhan 430070, P. R. China.
[*]E-mail: cai_haopeng@whut.edu.cn

Received: 14 June 2017 / *Accepted:* 12 July 2017 / *Published:* 13 August 2017

A facile method of pyrolysis of 2-methyl imidazole is used to prepare copper-doped iron carbide materials as counter electrodes for dye-sensitized solar cells. The content of copper in copper doped iron carbide materials are: 0.25%, 0.5%, 0.75%, 1% (molecular proportion). Among these DSSCs made from different Cu content Fe_3C cathodes, the Fe_3C-0.75%Cu based on the Cu content of 0.75% counter electrode yields the highest energy conversion efficiency of 5.68%. Compared to the Pt/C-based DSSC (6.22%), the DSSC fabricated from Fe_3C-0.75%Cu has a similar η. To evaluate the chemical catalysis of copper-doped iron carbide counter electrodes toward I_3^- reduction, cyclic voltammetry and electrochemical impedance spectra are carried out to characterize the counter electrodes. All the results have revealed that doped with copper can improve the catalytic ability of iron carbide counter electrodes. And the copper doped iron carbide counter electrode owns low prices of raw materials, simple production process, so it has very wide application prospects.

Keywords: copper-doped; iron carbide; counter electrodes; DSSC

1. INTRODUCTION

As the third-generation solar cells, dye-sensitized solar cells are widely concerned because of its low cost and high efficiency [1-3]. The counter electrode is an important part of the dye sensitized solar cells [4-6]. In the constituents of DSSC, the main function of the counter electrode is to catalyze the reduction of electrolyte solution and to collect electrons. Generally speaking, the counter electrode should have two advantages: high conductivity and high catalytic activity [7, 8]. Platinum is the most commonly used DSSC for the counter electrode catalytic materials due to its good stability and high electrocatalytic performance, but it is expensive, and the chemical stability of Pt is not satisfactory [9].

In order to solve this problem, it is urgent for us to seek some wide source, lower cost, better stability, and environmentally friendly materials to replace the metal counter electrode to fabricate Pt or reduce the dosage of platinum metal, and can maintain or exceed the excellent performance of electrode metal platinum.

Many materials such as carbon [10-17], copper oxide [18], transition metal nitride [19-21], transition metal sulfides [22], transition metal selenide [23-25], and composites [26-36] have been employed to replace Pt as the CE in DSSCs. Among these, transition metal carbides seem to be a brilliant substitute for its good catalytic activity, commendable thermal stability, especially low cost [37]. Transition metal carbides due to containing small carbon atom which inserted in the lattices so that behave outstanding catalytic activity. Guo et al. used metal chlorides and phenolic resin as source to prepare carbon supported WC, TiC and other transition metal carbide. These composites showed superior catalytic activities, the power conversion efficiencies of WC-C and TiC-C reached 9.42%, 8.85%, respectively [38]. Wu et al. through situ synthesis method prepared VC-MC (mesoporous carbon), which behaved a high power conversion efficiency of 7.63% [39]. Iron carbide (Fe_3C) seems more attractive for its abundance in the earth's crust and its high electronic conduction, higher resistance against oxidation and good catalytic activity as well. However, there is few work to study Fe_3C as the CE in DSSCs [40, 41].

In this article, we report a simple method for preparation of copper doped iron carbide successfully. The prepared material was used as counter electrode of DSSC, cyclic voltammetry and electrochemical impedance spectra were employed to evaluate its electrochemical behaviors.

2. EXPERIMENTAL SECTION

2.1. Chemicals.

Iron(III) chloride hexahydrate, Copper(II) Chloride Dihydrate, ethyl alcohol, 2-methyl imidazole, The redox shuttle electrolyte was composed of 10 mM LiI (anhydrous, 99%, Acros), 1 mM I_2 (anhydrous, 99.8%) and 0.1 M Lithium perchlorate (99%, Aldrich) in acetonitrile (99%, Fluka). All the chemicals were at least reagent grade and used as received without further purification.

2.2. Synthesis of iron carbide.

First of all, 0.01 mol Iron(III) chloride hexahydrate and 0.8 g 2-methyl imidazole were added into 37 mL ethyl alcohol to gain ferric chloride alcohol solution, stirring until all the solids are completely dissolved. After that the mixture was placed in the oil bath pot under stirring until the liquid evaporated completely at 80 ^oC. Grinding the remaining solid material for one minute, and the obtained composite was carbonized in N_2 at 900 ^oC atmosphere (The temperature of tube furnace rose from 0 ^oC to 900 ^oC and cooled down to room temperature naturally after 30 min, otherwise the rate was 180), then the Fe_3C was obtained.

2.3. Synthesis of copper doped Fe_3C Composite.

First, 0.01 mol Iron(III) chloride hexahydrate and Copper(II) Chloride Dihydrate (The molecular proportion of copper was 0.25, 0.5, 0.75, 1) and 0.8 g 2-methyl imidazole were added into 37 mL ethyl alcohol to gain ferric chloride alcohol solution, stirring until all the solids are completely dissolved. After that the mixture was placed in the oil bath pot under stirring until the liquid evaporated completely at 80 ^{o}C.Grinding the remaining solid material for one minute, and the obtained composite was carbonized in N_2 at 900 ^{o}C atmosphere (The temperature of tube furnace rose from 0 ^{o}C to 900 ^{o}C and cooled down to room temperature naturally after 30 min,otherwise the rate was 180), then the copper-doped iron carbide (Fe_3C-Cu) was obtained. The obtained Fe_3C-Cu with molecular proportion of Cu of 0.25, 0.5, 0.75, 1 were labeled as Fe_3C-0.25%Cu, Fe_3C-0.5%Cu, Fe_3C-0.75%Cu, Fe_3C-1%Cu.

2.4. Preparation of the counter electrodes

Respectively, quantity of four copper doped iron carbide 0.5 g sample was prepared, each with 2 ml NMP and a trace of PVDF, then put the samples in a mortar grinding for a while, let the mixture slightly adhesive, next put the samples in the ball milling speed in 180 rpm for 12 h, and finally get the copper doped iron carbide more viscous slurry.

2.5. Fabrication of the DSSCs

The electrode materials were dispersed in DMF by ultrasonication for 1 h, then casted on FTO conductive glass by spin-coating technique and heated at 80 °C for about 1 h to remove the solvent. the dye (N719)-absorbed anodes and counter electrodes were stacked and sealed with 60 μm thick thermal-plastic surlyn (DHS-SN1760) spacer at 110 ^{o}C for 15 s. An iodide-based liquid electrolyte (0.6 M DMPII, 0.03 M I2, 0.5 M TBP and 0.1 M LiI in MPN) was injected into the devices by capillary force.

2.6. Characterization.

The composition of the composite nanomaterials was characterized by X-ray diffraction (XRD) using a D/MAX-RB RU-200B diffractometer with Cu Kα (λ = 1.5406 Å) from 5 ^{o}C to 80 ^{o}C. The X-ray photoelectron spectroscopy (XPS) method (ESCALAB 250Xi) was used to verify the successful doping of copper in the samples. The scanning electron microscope (SEM) and transmission electron microscope (TEM) were used to characterize the morphology and structure of the samples. The cyclic voltammetry (CV) curves were carried out in a three-electrode system in a nitrogen-purged acetonitrile solution, which contains 0.1 M $LiClO_4$, 10 mM LiI and 1 mM I_2 with a scan rates 20 $mV{\cdot}s^{-1}$ in CHI660E electrochemical analyzer. Thereinto, Pt is worked as an auxiliary electrode, versus the Ag/Ag^{+} reference electrode. Electrochemical impedance spectroscopy (EIS) measurements were

performed using a Zahner Zennium electrochemical workstation by applying an AC voltage of 0.2 V amplitude in the frequency range between 10^6 Hz and 100 mHz with scan rate 5 $mV \cdot s^{-1}$ at room temperature. Photocurrent-voltage characteristics of the DSSCs were performed under simulated AM 1.5 G solar illumination. The intensity of incident solar illumination was adjusted to 100 mW/cm^2 using NREL-certified Si reference cell equipped with a KG-5 filter.

3. RESULTS AND DISCUSSION

Fig. 1(a) depicts the XRD patterns of Fe_3C samples, the major XRD diffraction peaks of Fe_3C appeared at 2θ=26.5°, 42.87°, 43.73°, 44.56°, 45.00°, 45.85°, 49.11°,corresponding to (002), (211), (102), (220), (031), (112), and (221) planes (JCPDS No. 85-1317). The diffraction peak of iron carbide is very strong, indicating a high degree of crystallinity, also shows that the iron carbide material was prepared successfully. The lattice constants are: a=5.0915 Å, b=6.7446 Å, c=4.5276 Å, the lattice volume is 0.15548 nm^3, the lattice density is 7.20 g/cm^3. Fig. 1b depicts the the diffraction peaks of Fe_3C-0.25%Cu around 2θ=39.78°, 42.87°, 43.74°, 44.55°, 44. 97°, 45.85°, 49.10°, corresponding to (002), (211), (102), (220), (031), (112), and (221) planes (JCPDS No.72-1110, 75-910, 85-1317). The lattice constants can be obtained as follows: a=5.0915 Å, b=6.7446 Å, c=4.5276 Å, the lattice size is 0.15548 nm^3, the lattice density is 7.20 g/cm^3. The diffraction peaks and planes of Fe_3C-0.5%Cu are the same as the Fe_3C-0.25%Cu. The diffraction peaks of Fe_3C-0.75%Cu around 2θ=37.75°, 42.89°, 43.75°, 44.57°, 44.99°, 45.87°, 49.12°, corresponding to (210), (211), (102), (220), (031), (112), and (221) planes (JCPDS No.72-1110, 75-0910, 76-1877, 77-0255, 85-0871). The lattice constants are a=5.0910 Å, b=6.7434 Å, c=4.5260 Å, and the lattice volume is 0.15538 nm^3, the lattice density is 7.24 g/cm^3. The diffraction peaks of Fe_3C-1%Cu around 2θ=39.78°, 42.87°, 43.74°, 44.55°, 44.97°, 45.85°, 49.10°, corresponding to (002), (211), (102), (220), (031), (112) and (221) planes (JCPDS No.72-1110, 75-910), and the lattice constant, volume and density are the same with Fe_3C-0.25%Cu. As can be seen from the figure, after doping with copper, a Fe_3C peak on the left becomes stronger. The XRD peak of Fe_3C-0.75%Cu shifts to the right, resulting in smaller lattice constants and higher density. This result is consistent with the reported XRD patterns for Fe3C without copper atoms in literature except the enhanced peak intensity[42].

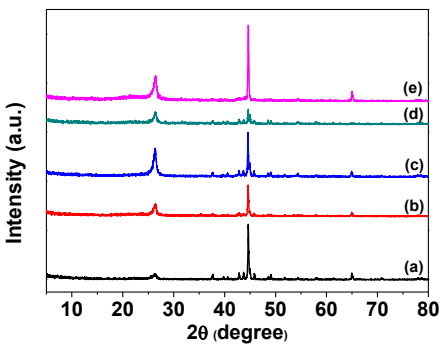

Figure 1. XRD patterns of (a) Fe_3C, (b) Fe_3C-0.25%Cu, (c) Fe_3C-0.5%Cu, (d) Fe_3C-0.75%Cu, (e) Fe_3C-1%Cu.

Fig 2(a) is the full spectrum of Fe_3C-0.25%Cu, Fe_3C-0.5%Cu, Fe_3C-0.75%Cu, Fe_3C-1%Cu. Fig 2(b, c) is the fitting of the iron and carbon atoms of Fe_3C-0.25%Cu, Fe_3C-0.5%Cu, Fe_3C-0.75%Cu, Fe_3C-1%Cu. Fig 2(d) is a copper atom spectrum. All the fitting graphs are corrected by using C1s as 284.8 eV. Based on the atomic occupying ratio calculation, and finally get the Fe_3C-0.75%Cu inside the copper and iron atoms was the highest. In the spectra of the copper atoms obtained by XPS test, there is no obvious strong peak and cannot be divided into peak fitting, but it can be seen in the Fig 2(a) that there are characteristic lines of Cu in the four samples proved the four kinds of copper atoms have been successfully doped into iron carbide.

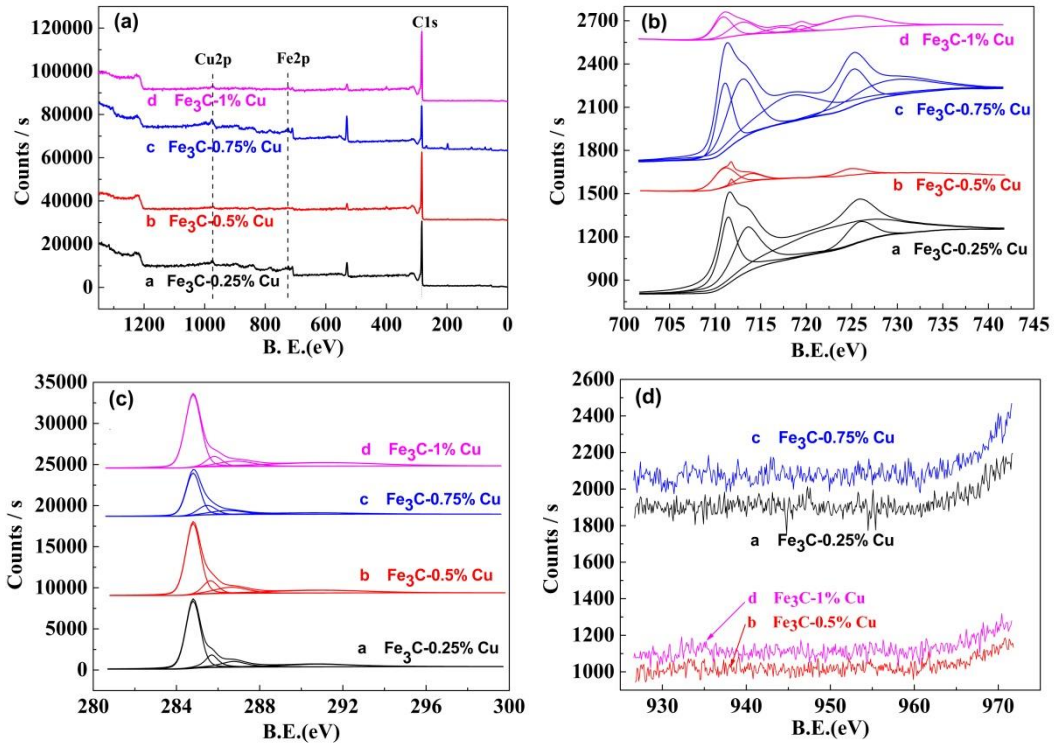

Figure 2. XPS spectra of Fe_3C-0.25%Cu, Fe_3C-0.5%Cu, Fe_3C-0.75%Cu, Fe_3C-1%Cu: (a) survey scans, (b) C 1s peak, (c) Fe 2p peak, (d) Cu 2p peak.

Fig 3 shows the SEM diagram of Fe_3C-0.25%Cu, Fe_3C-0.5%Cu, Fe_3C-0.75%Cu, Fe_3C-1%Cu. As shown in Fig 3(a, b) that the iron carbide materials have little difference and did not see a large lump proved that no agglomeration of iron carbide because of less copper atom content in Fe_3C-0.25%Cu and Fe_3C-0.5%Cu. Fig 3(c) indicates that the surface of Fe_3C-0.75%Cu has more fine particles and the porous structure is formed which is favorable to the penetration of the electrolyte so that redox reaction of the material becomes more quickly. Moreover, the structure has the advantages of larger surface area, better contact between the counter electrode material and the copper atom, thereby increasing the conductivity of the material, and the electrochemical performance of the material can be improved. Fig 3(d) shows that the particles of Fe_3C-1%Cu are large which may be caused by too many copper atoms and is unfavorable to the electrochemical catalytic activity of the material.

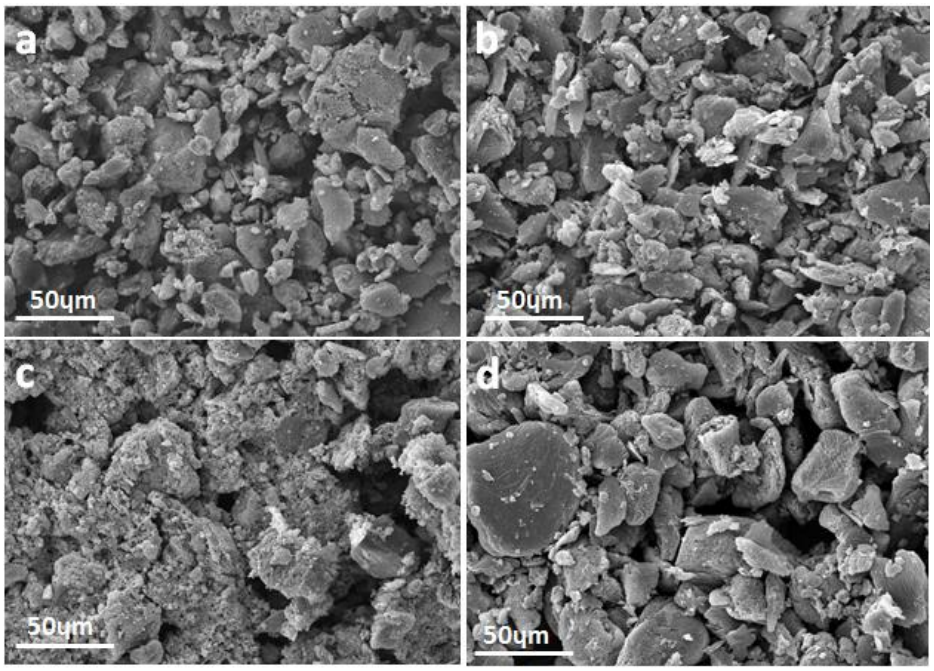

Figure 3. SEM images of counter electrodes: (a) Fe_3C-0.25%Cu, (b) Fe_3C-0.5%Cu, (c) Fe_3C-0.75%Cu, (d) Fe_3C-1%Cu.

Fig 4 shows the TEM diagram of Fe_3C-0.25%Cu, Fe_3C-0.5%Cu, Fe_3C-0.75%Cu and Fe_3C-1%Cu. The graph shows the particle size of Cu doped Fe_3C changes unapparent, copper atoms and iron carbide materials contact together closely which could reduce the resistance of charge in the transmission process. And the copper atoms dispersed in iron carbide materials, depending on the Cu content, the distribution is not the same.

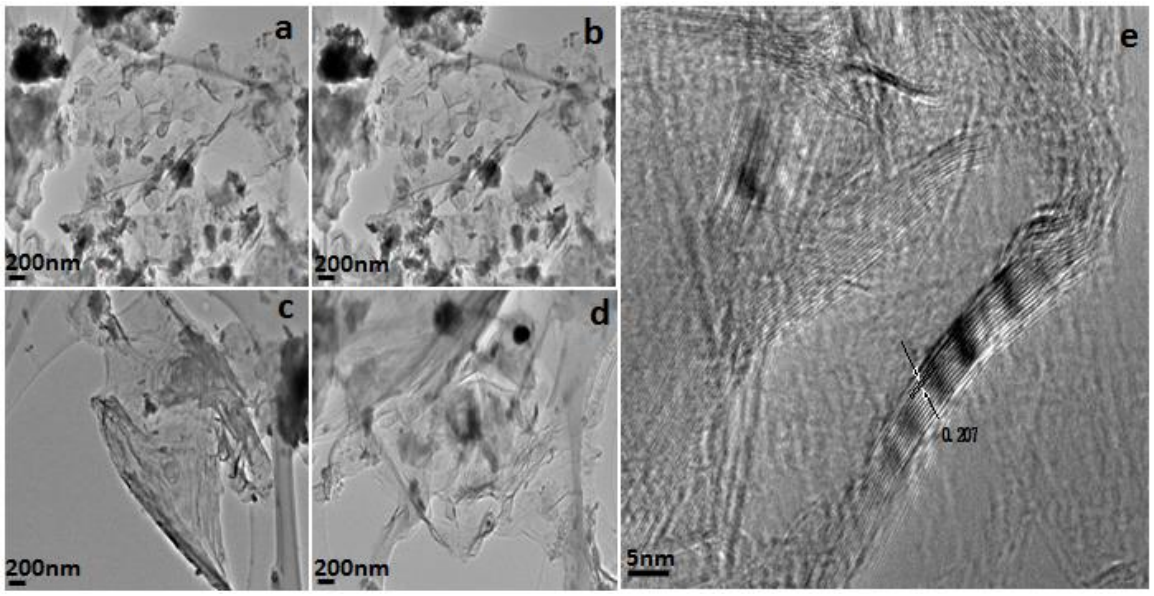

Figure 4. TEM images of counter electrodes: (a) Fe_3C-0.25%Cu, (b) Fe_3C-0.5%Cu, (c) Fe_3C-0.75%Cu, (d) Fe_3C-1%Cu, (e) HRTEM image of Fe_3C counter electrode.

Fig 4(a, b, d) show that copper atoms of Fe_3C-0.25%Cu, Fe_3C-0.5%Cu and Fe_3C-1%Cu have a small number of agglomeration which may have a certain impact on the charge transfer of the counter electrode material and hinder the diffusion of the electrolyte, leading to the reduction of the electrocatalytic properties of the materials. Fig 4(c) shows the copper atom of Fe_3C-0.75%Cu does not agglomerate and be able to observe the thin sheet structure of iron carbide material, these two phenomena will increase the contact area between the counter electrode and the electrolyte so as to improve the electrocatalytic performance and obtain higher photoelectric conversion efficiency. TEM shows that due to the doping of copper atoms, the particles of the Cu doped Fe_3C are closely linked and reduce the transmission resistance between electrons in the material so can improve the conductivity of the counter electrode materials. Fig 4(e) can be clearly observed that there are lattice fringes and the estimated crystal plane spacing is 0.207 nm, so it can be inferred from the corresponding is (102) plane. Fig 5 shows the CV curves of counter electrodes. Cyclic voltammetry (CV) was performed to evaluate the electrocatalytic activity of the counter electrodes to reduce triiodide using a three-electrode system. The scan rate of CV measurement has a great influence in the cathodic current density. The CV curves of counter electrodes were measured at the scan rate of 20 mV s^{-1}.

From Fig 5, it can be seen the CV curves of the CEs with Fe_3C-Cu display two pairs of redox peaks, indicating that they all possess electrocatalytic ability for the reduction of triiodide ions. The peak current of the reduction peak is usually used to characterize the electrochemical performance of the electrode, in the figure, when the copper content is 0.75%, the electrocatalytic activity of the electrode is higher. It can be concluded that the oxidation peak potential and the reduction peak potential difference of the Fe_3C-0.25%Cu, Fe_3C-0.5%Cu, Fe_3C-0.75%Cu and Fe_3C-1%Cu are respectively 0.437V, 0.41V, 0.319V, 0.398V. So the potential of Fe_3C-0.75%Cu has minimum difference. It can be seen from the graph that the current between the oxidation peak potential and the reduction peak potential with the voltage is linear relationship, so the reversibility of the electrode is the best. The possible reason is due to the addition of Cu atoms, exists a number of Cu^{2+} in iron carbide crystals, the presence of these ions will increase the conductivity of the whole material, the counter electrode has better catalytic activity and reversibility.

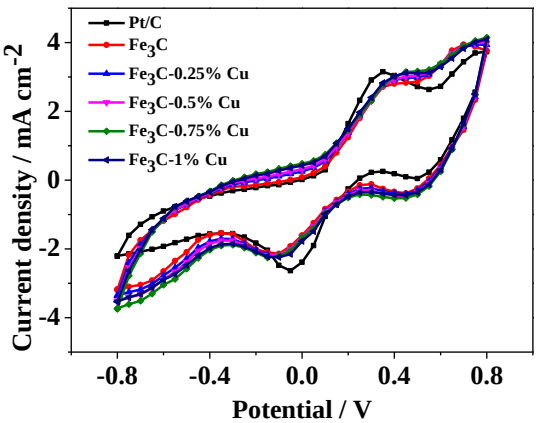

Figure 5. Cyclic voltammograms for the cathodes at a scan rate of 20 mV s^{-1} in 10 mM LiI, 1 mM I_2 acetonitrile solution containing 0.1M $LiClO_4$ as the supporting electrolyte.

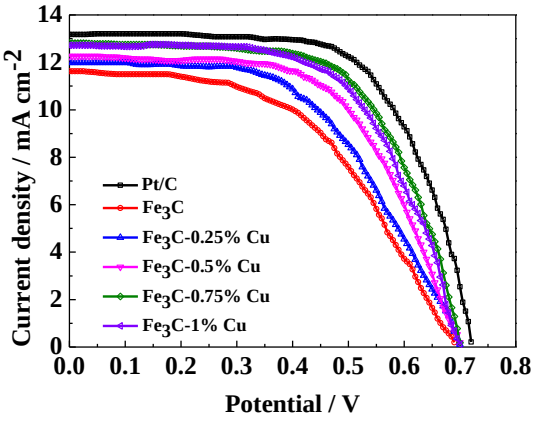

Figure 6. Typical photocurrent-photovoltage curves of DSSCs based on Fe_3C-0.25%Cu, Fe_3C-0.5%Cu,Fe_3C-0.75%Cu, Fe_3C-1%Cu, Fe_3C and Pt counter electrodes.

When the amount of Cu is too small, the content of Cu^{2+} generates too little, properties of counter electrode materials have not been too much improved; but when the concentration is too high, causes iron carbide blocking and hinder ion transfer, resulting in a decline in performance of counter electrode materials, so only when the Cu content is moderate, the material on the counter electrode performs best.

Table 1. Detailed Photovoltaic Parameters for DSSCs Fabricated with Different Cathodes

cells	V_{oc}(V)	J_{sc}(mAcm^{-2})	FF(%)	η(%)
Fe_3C-0.25%Cu	0.7	11.99	0.53	4.45
Fe_3C-0.5%Cu	0.7	12.26	0.59	5.07
Fe_3C-0.75%Cu	0.7	12.81	0.63	5.68
Fe_3C-1%Cu	0.7	12.72	0.61	5.46
Fe_3C	0.69	11.62	0.51	4.07
Pt	0.72	13.17	0.65	6.22

"J_{sc}, short-circuit photocurrent; V_{oc}, open-circuit photovoltage; FF, fill factor; η, energy conversion efficiency.

Fig 6 shows the J-V curves of the DSSCs assembled based on Fe_3C-0.25%Cu, Fe_3C-0.5%Cu, Fe_3C-0.75%Cu, Fe_3C-1%Cu, Fe_3C and Pt counter electrodes. All of the counter electrodes are measured under the illumination of 1 sun (100 mW cm-2). The photovoltaic parameters of these devices, including the open circuit voltage(Voc), the short-circuit photocurrent density (J_{sc}), the fill factor (FF) and the energy conversion efficiency (η), are summarized in Table 1. The J_{sc} and FF complied with the order Fe_3C-0.75%Cu > Fe_3C-1%Cu > Fe_3C-0.5%Cu > Fe_3C-0.25%Cu > Fe_3C. The DSSC with Fe_3C-0.75%Cu counter electrode exhibits a relatively higher η. The Fe_3C-0.25%Cu, Fe_3C-0.5%Cu, Fe_3C-0.75%Cu, Fe_3C-1%Cu and Fe_3C give η of 4.45%, 5.07%, 5.68%, 5.46% and 4.07%, respectively. The DSSC with Fe_3C-0.75%Cu counter electrode possesses the best energy conversion efficiencies of 5.68% among the DSSCs with Fe_3C and Cu doped Fe_3C counter electrodes. It should be

mentioned that the energy conversion efficiency is somewhat lower than that reported in literature for Fe_3C/nitrogen-doped carbon system[43] and Fe_3W_3C/graphite carbon system[44] due to the different composition of the applied materials. However, the relatively simple synthetic process makes the reported materials in this paper practically applicable for DSSCs.

Fig 7 shows the EIS spectra of the counter electrodes. The electrochemical impedance spectroscopy of dye-sensitized solar cells was carried out on CHI660, and the test frequency was 5 mV/s, The equivalent circuit diagram as follows:

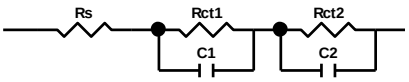

Among them, Rs is the contact resistance, it is the value of the corresponding impedance curve and the real axis intercept; R_{ct1} is the resistance between the counter electrode and the electrolyte, can be obtained by calculating the diameter of the first semicircle; R_{ct2} is the interface resistance between anode and electrolyte, can be obtained by calculating the diameters of second semicircle. The smaller the value of R_{ct1}, the better the performance of the counter electrode material.

Table 2. Detailed EIS Parameters for DSSCs with Fe_3C-0.25%Cu, Fe_3C-0.5%Cu, Fe_3C-0.75%Cu, Fe_3C-1%Cu, Fe_3C and Pt counter electrodes.

cells	$R_s(\Omega)$	$R_{ct}(\Omega)$	$R_{ct2}(\Omega)$
Fe_3C-0.25%Cu	0.219	5.688	3.063
Fe_3C-0.5%Cu	0.155	5.341	3.415
Fe_3C-0.75%Cu	0.158	5.004	3.199
Fe_3C-1%Cu	0.146	5.054	3.231
Fe_3C	0.415	7.300	2.181
Pt	0.119	4.378	2.799

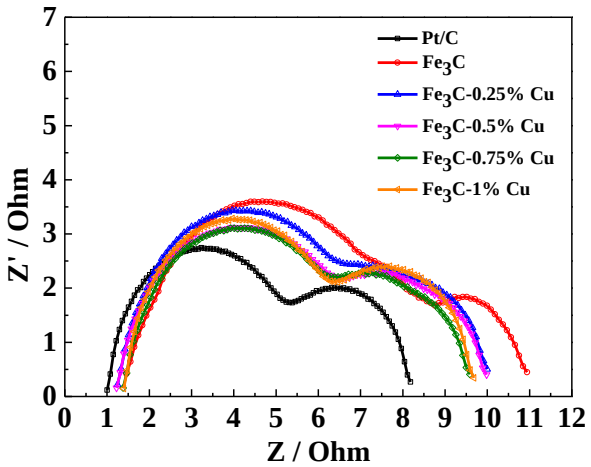

Figure 7. Nyquist plots of the Fe_3C-0.25%Cu, Fe_3C-0.5%Cu, Fe_3C-0.75%Cu, Fe_3C-1%Cu, Fe_3C and Pt DSSCs.

It can be seen from the figure that with the increase of Cu content, R_{ct1} decreases gradually, shows that the conductive property of the counter electrode increases, probably due to Cu has excellent conductive properties, and it is dispersed uniformly in Fe_3C, facilitates the transfer between electric charges, the overall conductivity of the material is improved. And indicates that with the increase of Cu, the capacitance characteristic of the material becomes better, but too much Cu will decrease the performance. The simulated charge-transfer resistances of Fe_3C-0.25%Cu, Fe_3C-0.5%Cu, Fe_3C-0.75%Cu, Fe_3C-1%Cu and Fe_3C counter electrodes are 5.688 Ω, 5.341 Ω, 5.004 Ω, 5.054 Ω and 7.3 Ω respectively. The Fe_3C-0.75%Cu DSSC has the smallest R_{ct1} among the Fe_3C and the Cu doped Fe_3C DSSCs.

4. CONCLUSIONS

In this paper, copper doped iron carbide material was synthesized by simple method as counter electrodes for dye-sensitized solar cell, in which carbon source for 2-methyl imidazole. Among these DSSCs made from different Cu content Fe_3C cathodes, the Fe_3C-0.75%Cu yields the highest energy conversion efficiency of 5.68%, that mainly due to the DSSC with Fe_3C-0.75%Cu counter electrode has the faster electron transfer and higher catalytic performance, and it also has the lower interfacial transfer resistance.

ACKNOWLEDGEMENTS
This work was financially supported by the National Nature Science Foundation of China (61376064).

References

1. B. O'Regan, M. Grätzel, Nature, 353 (1991) 737.
2. P. Allongue, E. Souteyrand, Journal of Electroanalytical Chemistry, 362 (1993) 79.
3. D. Chapin, J. Appl. Phys.; (United States), 25 (1954).
4. N.R. Neale, N. Kopidakis, J.V.D. Lagemaat, M. Grätzel, A.J. Frank, Journal of Physical Chemistry B, 109 (2005) 23183.
5. T. Çaykara, S. Demirci, M.S. Eroğlu, O. Güven, Polymer, 46 (2005) 10750-10757.
6. M.S. Akhtar, K.K. Cheralathan, J.M. Chun, O.B. Yang, Electrochimica Acta, 53 (2008) 6623.
7. T.N. Rao, L. Bahadur, Journal of the Electrochemical Society, 144 (1996) 179.
8. J. Moser, M. Grätzel, Chimia International Journal for Chemistry, 52 (1998) 160.
9. J. Halme, M. Toivola, A. Tolvanen, P. Lund, Solar Energy Materials & Solar Cells, 90 (2006) 872.
10. S.A.S. †, C.M.E. †, ,, Cristiano Contado, A. Stefano Caramori, C.A.B. ‡, Journal of the American Chemical Society, 124 (2002) 11215.
11. X. Fang, T. Ma, G. Guan, M. Akiyama, T. Kida, E. Abe, Journal of Electroanalytical Chemistry, 570 (2004) 257.
12. A. Kay, M. Grätzel, Solar Energy Materials & Solar Cells, 44 (1996) 99-.
13. E. Olsen, G. Hagen, S.E. Lindquist, Solar Energy Materials & Solar Cells, 63 (2000) 267.
14. H. Ago, K. Petritsch, M.S.P. Shaffer, A.H. Windle, R.H. Friend, Advanced Materials, 11 (1999) 1281.
15. H.S. Wroblowa, A. Saunders, Journal of Electroanalytical Chemistry & Interfacial Electrochemistry, 42 (1973) 329.
16. B.E. Conway, J.O.M. Bockris, R.E. White, Modern Aspects of Electrochemistry, Plenum Press, 1989.

17. Z. Huang, X. Liu, K. Li, D. Li, Y. Luo, H. Li, W. Song, L.Q. Chen, Q. Meng, Electrochemistry Communications, 9 (2007) 596.
18. S. Anandan, X. Wen, S. Yang, Materials Chemistry & Physics, 93 (2005) 35.
19. Q.W. Jiang, G.R. Li, X.P. Gao, Chemical Communications, 44 (2009) 6720.
20. H. Tang, Y. Zeng, D. Liu, D. Qu, J. Luo, K. Binnemans, D.E. De Vos, J. Fransaer, D. Qu, S.-G. Sun, Nano Energy, 26 (2016) 131.
21. X. Zhang, X. Chen, S. Dong, Z. Liu, X. Zhou, J. Yao, S. Pang, H. Xu, Z. Zhang, L. Li, Journal of Materials Chemistry, 22 (2012) 6067.
22. V.P.S. Perera, P.K.D.D.P. Pitigala, P.V.V. Jayaweera, K.M.P. Bandaranayake, K. Tennakone, J.phys.chem.b, 107 (2003) 13758.
23. F. Gong, H. Wang, X. Xu, G. Zhou, Z.S. Wang, Journal of the American Chemical Society, 134 (2012) 10953.
24. F. Gong, X. Xu, Z. Li, G. Zhou, Z.S. Wang, Chemical Communications, 49 (2013) 1437.
25. Z. Zhang, S. Pang, H. Xu, Z. Yang, X. Zhang, Z. Liu, X. Wang, X. Zhou, S. Dong, X. Chen, Rsc Advances, 3 (2013) 16528.
26. H. Bi, W. Zhao, S. Sun, H. Cui, T. Lin, F. Huang, X. Xie, M. Jiang, Carbon, 61 (2013) 116.
27. H. Cai, J. Li, X. Xu, H. Tang, J. Luo, K. Binnemans, J. Fransaer, D.E. De Vos, Journal of Alloys and Compounds, 697 (2017) 132.
28. J.Y. Lin, G. Yue, S.Y. Tai, Y. Xiao, H.M. Cheng, F.M. Wang, J. Wu, Materials Chemistry & Physics, 143 (2013) 53.
29. J.Y. Lin, C.Y. Chan, S.W. Chou, Chemical Communications, 49 (2013) 1440.
30. G. Yue, J. Wu, J.Y. Lin, Y. Xiao, S.Y. Tai, J. Lin, M. Huang, Z. Lan, Carbon, 55 (2013) 1.
31. S.Y. Tai, C.J. Liu, S.W. Chou, S.S. Chien, J.Y. Lin, T.W. Lin, Journal of Materials Chemistry, 22 (2012) 2475.
32. J. Song, G.R. Li, F.Y. Xiong, X.P. Gao, Journal of Materials Chemistry, 22 (2012) 20580.
33. L. Yi, Y. Liu, N. Yang, Z. Tang, H. Zhao, G. Ma, Z. Su, D. Wang, Energy & Environmental Science, 6 (2013) 835.
34. S. Yun, H. Zhang, H. Pu, J. Chen, A. Hagfeldt, T. Ma, Advanced Energy Materials, 3 (2013) 1407.
35. Y. Peng, J. Zhong, K. Wang, B. Xue, Y.B. Cheng, Nano Energy, 2 (2013) 235.
36. H. Zheng, C.Y. Neo, J. Ouyang, Acs Applied Materials & Interfaces, 5 (2013).
37. S. Thomas, T.G. Deepak, G.S. Anjusree, T.A. Arun, S.V. Nair, A.S. Nair, J. Mater. Chem. A, 2 (2014) 4474.
38. H. Guo, Q. Han, C. Gao, H. Zheng, Y. Zhu, M. Wu, Journal of Power Sources, 332 (2016) 399.
39. M. Wu, X. Lin, Y. Wang, L. Wang, W. Guo, D. Qi, X. Peng, A. Hagfeldt, M. Gratzel, T. Ma, J Am Chem Soc, 134 (2012) 3419.
40. H.X. Xu, C.J. Zhang, Z.W. Wang, S.P. Pang, X.H. Zhou, Z.Y. Zhang, G.L. Cui, Journal of Materials Chemistry A, 2 (2014) 4676.
41. Y.P. Liao, K. Pan, L. Wang, Q.J. Pan, W. Zhou, X.H. Miao, B.J. Jiang, C.G. Tian, G.H. Tian, G.F. Wang, H.G. Fu, Acs Applied Materials & Interfaces, 5 (2013) 3663.
42. Y. Gu, M. Qin, Z. Cao, B. Jia, X. Wang, X. Qu, Journal of the American Ceramic Society, 99 (2016) 1443.
43. H. Xu, C. Zhang, Z. Wang, S. Pang, X. Zhou, Z. Zhang, G. Cui, Journal of Materials Chemistry A, 2 (2014) 4676.
44. Y. Liao, Y. Xie, K. Pan, G. Wang, Q. Pan, W. Zhou, L. Wang, B. Jiang, H. Fu, Chemsuschem, 8 (2015) 726.